Nanoscale Advances

COMMUNICATION

View Article Online
View Journal | View Issue

Cite this: *Nanoscale Adv.*, 2019, **1**, 961

Enabling the electrocatalytic fixation of N_2 to NH_3 by C-doped TiO_2 nanoparticles under ambient conditions†

Kun Jia,[ab] Yuan Wang,[ab] Qi Pan,[ab] Benhe Zhong,[a] Yonglan Luo,[b] Guanwei Cui,[c] Xiaodong Guo*[a] and Xuping Sun *[b]

Received 22nd October 2018
Accepted 19th November 2018

DOI: 10.1039/c8na00300a

rsc.li/nanoscale-advances

The conventional Haber–Bosch process for industrial NH_3 production from N_2 and H_2 is highly energy-intensive with a large amount of CO_2 emissions and finding a more suitable method for NH_3 synthesis under mild conditions is a very attractive topic. The electrocatalytic N_2 reduction reaction (NRR) offers us an environmentally benign and sustainable route. In this communication, we report that C-doped TiO_2 nanoparticles act as an efficient electrocatalyst for the NRR with excellent selectivity. In 0.1 M Na_2SO_4, it achieves an NH_3 yield of 16.22 μg h^{-1} $mg_{cat.}^{-1}$ and a faradaic efficiency of 1.84% at −0.7 V *vs.* the reversible hydrogen electrode. Furthermore, this catalyst also shows good stability during electrolysis and recycling tests.

NH_3 is an essential ingredient in the manufacture of fertilizers, medicaments, resins, dyes, explosives, *etc.*[1–4] In 2017, total worldwide NH_3 production exceeded 150 million tons, and the demand for NH_3 continues to grow.[5] Industrially, NH_3 is produced almost *via* the Haber–Bosch process.[6] In order to overcome the kinetic limitations of strong N≡N triple bonds, elevated temperature (350–550 °C) and high pressure (150–350 atm) are necessary throughout the whole process.[7–9] Moreover, it not only consumes a large amount of energy, but inevitably leads to significant CO_2 emission. So, it is imperative to develop an environmentally friendly process for the sustainable conversion of N_2 to NH_3.

Electrochemical NH_3 synthesis from N_2 and H_2O is a promising candidate for artificial N_2 fixation under ambient conditions due to its environment-friendly, convenient and low-cost characteristics.[10–15] Although electrochemical reduction is feasible for achieving the conversion of N_2 to NH_3, it requires electrocatalysts for the N_2 reduction reaction (NRR) to meet the challenge associated with N_2 activation. Noble-metal catalysts such as Ru,[16] Au,[17,18] Ag,[19] and Rh[20] were reported as NRR catalysts with attractive catalytic performances, but the scarcity of these catalysts limits their wide application. Recently, transition metal oxides (TMOs)[21–26] have attracted much attention as NRR electrocatalysts, as they are inexpensive and can be easily prepared on a large scale. Therefore, it is still highly desirable to develop TMOs for the NRR. TiO_2 is nontoxic with a high thermal stability,[27] but its low electronic conductivity hinders its electrocatalytic application.[28] It has been reported that carbon doping can enhance the electronic conductivity of TiO_2 and facilitate charge transfer from the bulk to the surface region,[29] offering us a possible catalyst for the NRR, which, however, has not been explored before.

Herein, we report that C-doped TiO_2 nanoparticles (C-TiO_2) are effective for electrochemical N_2 conversion to NH_3 with excellent selectivity under ambient conditions. In 0.1 M Na_2SO_4, the catalyst achieves an NH_3 yield of 16.22 μg h^{-1} $mg_{cat.}^{-1}$ and a faradaic efficiency (FE) of 1.84% at −0.7 V *vs.* the reversible hydrogen electrode (RHE). Remarkably, it also demonstrates a high electrochemical stability. Compared with pristine TiO_2 (NH_3 yield: 8.49 μg h^{-1} $mg_{cat.}^{-1}$; FE: 1.28%), C-TiO_2 has a superior NRR performance. This result suggests that the introduction of carbon can enhance the electrocatalytic activity of TiO_2.

C-TiO_2 nanoparticles were prepared by a facile calcination assisted solvothermal method (see the ESI† for preparation details). Fig. 1a presents the X-ray diffraction (XRD) patterns of C-TiO_2 and TiO_2. The diffraction peaks at 25.3°, 37.8°, 48.0°, 53.9°, 55.1°, and 62.7° can be indexed to the (101), (004), (200), (105), (211), and (204) planes of anatase TiO_2 (JCPDS no. 21-1272), respectively, which is similar to the pattern of C-TiO_2. Thermal gravimetric analysis (Fig. S1†) demonstrated that the content of C was 2.97 wt%. Scanning electron microscopy (SEM) images (Fig. S2†) indicate that the crystallite size of C-TiO_2 is smaller than that of TiO_2. Fig. 1b shows a transmission electron microscopy (TEM) image which evidences the nanoparticle

[a]School of Chemical Engineering, Sichuan University, Chengdu 610065, China. E-mail: xiaodong2009@scu.edu.cn
[b]Institute of Fundamental and Frontier Sciences, University of Electronic Science and Technology of China, Chengdu 610054, China. E-mail: xpsun@uestc.edu.cn
[c]College of Chemistry, Chemical Engineering and Materials Science, Shandong Normal University, Jinan 250014, Shandong, China

† Electronic supplementary information (ESI) available: Experimental section and supplementary figures. See DOI: 10.1039/c8na00300a

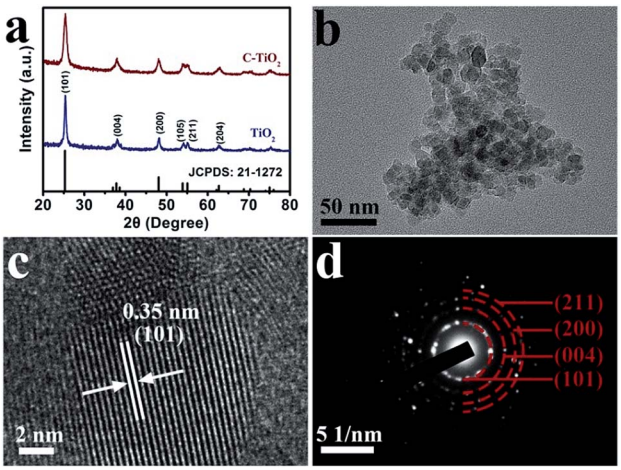

Fig. 1 (a) XRD patterns for C-TiO_2 and TiO_2. (b) TEM and (c) HRTEM images for the C-TiO_2 nanoparticles. (d) SAED pattern for C-TiO_2.

nature of C-TiO_2. A high-resolution TEM (HRTEM) image (Fig. 1c) reveals a well-resolved lattice fringe with an interplanar distance of 0.35 nm, indexed to the (101) plane of C-TiO_2. The selected area electron diffraction (SAED) pattern of C-TiO_2 (Fig. 1d) exhibited four diffraction rings indexed to the (101), (004), (200) and (211) planes of the TiO_2 phase.

Fig. 2a shows the X-ray photoelectron spectroscopy (XPS) survey spectrum of C-TiO_2, which confirms the presence of Ti, C, and O elements. Fig. 2b presents the Ti 2p spectra for the C-TiO_2 and TiO_2 samples. The binding energies (BEs) of Ti $2p_{3/2}$ and Ti $2p_{1/2}$ for TiO_2 are 458.38 and 464.07 eV, respectively.[30] Compared to the TiO_2 sample, the Ti 2p peaks of C-TiO_2 show a positive shift of 0.3 eV, which could be attributed to lattice distortions.[31] Fig. 2c reveals the O 1s spectra for C-TiO_2 which are in good agreement with those of pure TiO_2. The BEs at 529.92 and 531.33 eV in the O 1s region are ascribed to the Ti–O–Ti (lattice oxygen) and O–H bonds in C-TiO_2.[32,33] For the C 1s XPS spectra (Fig. 2d), three peaks can be deconvoluted at around 284.76, 286.15, and 289.12 eV for C-TiO_2. The peak at 284.76 eV could be attributed to the surface adventitious carbon.[30] The two peaks at 286.15 and 289.12 eV are characteristic of the oxygen bound species C–O and Ti–O–C, respectively.[34] This result indicates that carbon atoms substitute for some of the lattice titanium atoms and form a Ti–O–C structure.[30] Compared with C-TiO_2, only one C 1s XPS spectrum corresponding to C–C is observed for the TiO_2 sample, further confirming the existence of C in C-TiO_2. In addition, the ultraviolet-visible (UV-vis) absorption spectra and the corresponding Kubelka–Munk plots of C-TiO_2 and TiO_2 are displayed in Fig. S3.† The band gap energies of C-TiO_2 (2.79 eV) and TiO_2 (2.96 eV) were determined by the intercept of the plots of $(\alpha h\nu)^{1/2}$ *versus* photon energy ($h\nu$),[35] indicating a narrower band gap after C doping. The enhancement of visible light absorption for C-TiO_2 and TiO_2 should be attributed to the carbon doping in the TiO_2 lattice, which would introduce a series of localized occupied states into the band gap of the TiO_2 lattice, leading to a strong visible light absorption.[36] All of the above results strongly support the successful preparation of C-TiO_2 nanoparticles.

The electrocatalytic NRR performance of C-TiO_2 was tested using a typical two-compartment and three-electrode device as the reaction vessel. C-TiO_2 was deposited on carbon paper (C-TiO_2/CP with a C-TiO_2 loading of 0.10 mg) for the test. All of the potentials for the NRR were reported on the RHE scale. The produced NH_3 was detected by spectrophotometry with salicylic acid.[37] The relevant calibration curves are shown in Fig. S4.† The chronoamperometry curves at the corresponding potentials in N_2-saturated 0.1 M Na_2SO_4 are displayed in Fig. 3a, which can directly express the relationship between current density and time during the whole test process. Fig. 3b presents the UV-vis absorption spectra of the electrolyte stained with indophenol indicator after 2 h electrolysis at a series of potentials, and the

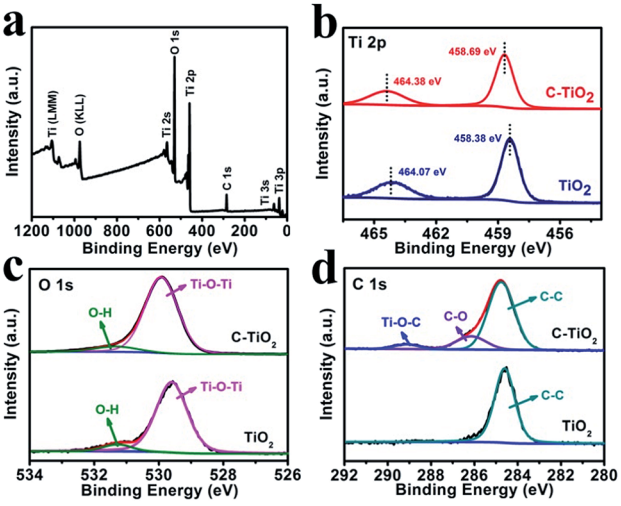

Fig. 2 (a) XPS survey spectrum for C-TiO_2. XPS spectra of C-TiO_2 and TiO_2 in the (b) Ti 2p, (c) O 1s and (d) C 1s regions.

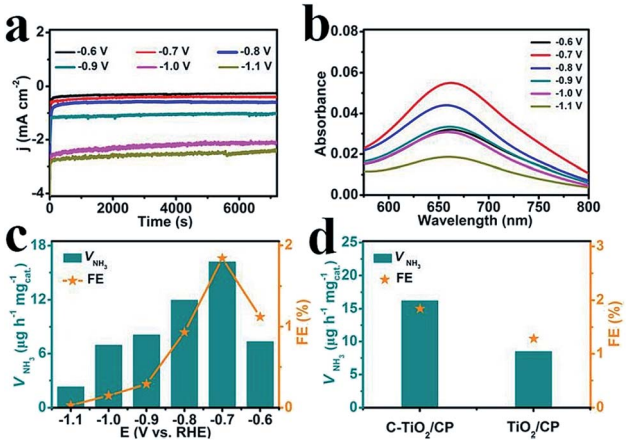

Fig. 3 (a) Chronoamperometry curves at the corresponding potentials in N_2-saturated 0.1 M Na_2SO_4. (b) UV-vis absorption spectra of the electrolytes stained with indophenol indicator after 2 h electrolysis at a series of potentials. (c) The NH_3 yields and FEs of C-TiO_2 for the NRR at a series of potentials. (d) The amount of NH_3 with different electrodes at −0.7 V after 2 h electrolysis under ambient conditions.

values of absorbance at 660 nm were used to calculate the concentrations of the generated NH_3 at different applied potentials according to the calibration curve of NH_3. Combined with the collected data, the final results including the NH_3 yields and FEs under various potentials were calculated and are plotted in Fig. 3c. Both the NH_3 yields and FEs increase as the negative potential rises to −0.7 V, which is the optimum potential point when the NH_3 yield and FE are 16.22 μg h^{-1} $mg_{cat.}^{-1}$ and 1.84%, respectively. After that, as the potential continually increases, both the NH_3 yields and FEs decrease significantly which is mainly caused by the competitive hydrogen evolution reaction. For comparison, the pure TiO_2 sample was tested under the same conditions and the corresponding results are presented in Fig. 3d. It is worth noting that the performance of C-TiO_2 is evidently better than that of pure TiO_2. The superior NRR performance of C-TiO_2 can be rationally attributed to the C-TiO_2 nanoparticles having more exposed active sites (Fig. S5†), enabling more effective utilization of them as electrocatalysts. The enhanced conductivity of C-TiO_2 also contributes to its higher catalytic activity. The charge transfer resistance related to the electrocatalytic kinetics can be determined from the diameter of the semicircles in the low frequency zone.[38] Electrochemical impedance spectroscopy data (Fig. S6†) show that C-TiO_2/CP possesses a smaller radius of the semicircle compared to TiO_2/CP, suggesting that the C-TiO_2 sample has a lower charge transfer resistance[39] and thus faster NRR kinetics. Meanwhile, C-TiO_2 shows a higher performance than some of the previously reported NRR electrocatalysts.[40–44] More detailed comparisons are listed in Table S1.†

To prove that NH_3 was generated *via* the N_2 reduction process of C-TiO_2, three sets of control experiments were carried out: (1) immersing the samples in Ar-saturated solution at −0.7 V for 2 h; (2) immersing the samples in N_2-saturated solution at an open circuit potential for 2 h; and (3) immersing the samples at −0.7 V with alternating 2 h cycles between N_2-saturated and Ar-saturated solutions, for a total of 12 h. As shown in Fig. 4a and Fig. S7,† a trace amount of NH_3 production was detected under Ar-saturated solution and an open circuit potential. Combined with Fig. S8,† this result indicates that only N_2 provides the nitrogen source to NH_3. Moreover, controlled trials were carried out to investigate the performance of bare CP. The relevant UV-vis absorption spectra are displayed in Fig. S9.† The results show the poor electrocatalytic activity of bare CP, indicating that C-TiO_2 is an active material for the NRR (Fig. 4b). In addition, stable performance is another important indicator for evaluating catalysts. Recycling tests were performed in N_2-saturated 0.1 M Na_2SO_4 6 times and the results are shown in Fig. 4c. The NH_3 yield and FE results show no obvious fluctuation over the whole process, suggesting that C-TiO_2 possesses a stable NRR performance. Moreover, only a slight fluctuation of current density is observed at −0.7 V after 24 h electrolysis, further suggesting an excellent electrochemical stability.

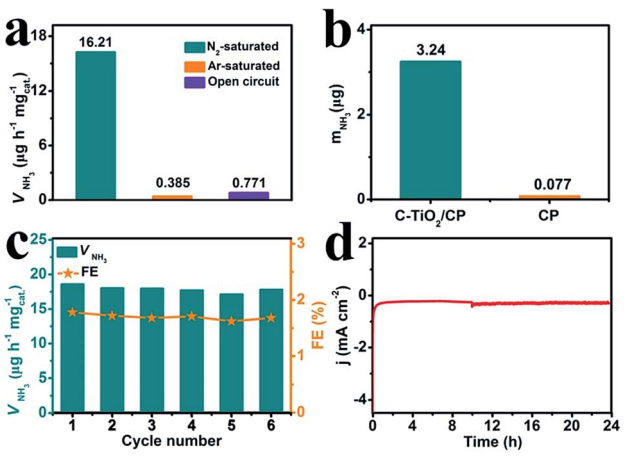

Fig. 4 (a) NH_3 yields for C-TiO_2 under different conditions. (b) The amount of NH_3 with different electrodes at −0.7 V after 2 h electrolysis under ambient conditions. (c) NH_3 yields and FEs at a potential of −0.7 V during 6 recycling tests. (d) Chronoamperometry curve at a potential of −0.7 V using a C-TiO_2/CP catalyst for 24 h.

Hydrazine (N_2H_4), as a possible by-product in the NRR test, was detected by the method of Watt and Chrisp.[45] The relevant calibration curves are displayed in Fig. S10.† The UV-vis absorption spectra of N_2H_4 after 2 h electrolysis in a N_2 atmosphere at a series of potentials are shown in Fig. S11.† The concentrations of the possible by-product N_2H_4 are determined according to the values of absorbance at 455 nm. The results demonstrated that no N_2H_4 was detected at all potentials, implying the excellent selectivity of C-TiO_2 as an NRR electrocatalyst.

In summary, C-TiO_2 nanoparticles have been proven as an effective non-noble-metal electrocatalyst for the NRR at moderate temperatures and atmospheric pressure. This electrocatalyst achieves an NH_3 yield of 16.22 μg h^{-1} $mg_{cat.}^{-1}$ and a FE of 1.84% at −0.7 V *vs.* RHE in 0.1 M Na_2SO_4. It also exhibits excellent selectivity and satisfactory electrochemical stability during the process of electrochemical NH_3 synthesis under ambient conditions. This work not only offers us an attractive earth-abundant electrocatalyst for the NRR, but also opens up an exciting new avenue for the design and development of doped Ti-based catalysts[46,47] with enhanced performances toward electrocatalytic N_2 and nitrite[48] reduction for applications.

Conflicts of interest

There are no conflicts to declare.

Acknowledgements

The authors would like to thank the National Natural Science Foundation of China (No. 21506133) and the Youth Foundation of Sichuan University (No. 2017SCU04a08) for their support in this research.

References

1 R. Schlögl, *Angew. Chem., Int. Ed.*, 2003, **42**, 2004–2008.

2 T. Murakami, T. Nishikiori, T. Nohira and Y. Ito, *J. Am. Chem. Soc.*, 2003, **125**, 334–335.
3 V. Rosca, M. Duca, M. T. de Groot and M. T. Koper, *Chem. Rev.*, 2009, **109**, 2209–2244.
4 C. Guo, J. Ran, A. Vasileff and S. Qiao, *Energy Environ. Sci.*, 2018, **11**, 45–56.
5 J. A. Ober, *Mineral Commodity Summaries 2018*, ed. S. M. Kimball, U.S. Geological Survey, U.S. Government Printing Office, Washington, DC, 2018, DOI: 10.3133/70194932.
6 V. Smil, *Nature*, 1999, **400**, 415.
7 G. Ertl, *Catalytic ammonia synthesis*, ed. J. R. Jennings, Plenum, New York, 1991.
8 C. J. M. van der Ham, M. T. M. Koper and D. G. H. Hetterscheid, *Chem. Soc. Rev.*, 2014, **43**, 5183–5191.
9 G. Chen, X. Cao, S. Wu, X. Zeng, L. Ding, M. Zhu and H. Wang, *J. Am. Chem. Soc.*, 2017, **139**, 9771–9774.
10 L. Zhang, X. Ji, X. Ren, Y. Ma, X. Shi, Z. Tian, A. M. Asiri, L. Chen, B. Tang and X. Sun, *Adv. Mater.*, 2018, **30**, 1800191.
11 X. Ren, G. Cui, L. Chen, F. Xie, Q. Wei, Z. Tian and X. Sun, *Chem. Commun.*, 2018, **54**, 8474–8477.
12 L. Zhang, X. Ji, X. Ren, Y. Luo, X. Shi, A. M. Asiri, B. Zheng and X. Sun, *ACS Sustainable Chem. Eng.*, 2018, **6**, 9550–9554.
13 X. Li, T. Li, Y. Ma, Q. Wei, W. Qiu, H. Guo, X. Shi, P. Zhang, A. M. Asiri, L. Chen, B. Tang and X. Sun, *Adv. Energy Mater.*, 2018, **8**, 1801357.
14 W. Qiu, X. Xie, J. Qiu, W. Fang, R. Liang, X. Ren, X. Ji, G. Cui, A. M. Asiri, G. Cui, B. Tang and X. Sun, *Nat. Commun.*, 2018, **9**, 3485.
15 R. Zhang, Y. Zhang, X. Ren, G. Cui, A. M. Asiri, B. Zheng and X. Sun, *ACS Sustainable Chem. Eng.*, 2018, **6**, 9545–9549.
16 V. Kordali, G. Kyriacou and C. Lambrou, *Chem. Commun.*, 2000, **17**, 1673–1674.
17 M. Shi, D. Bao, B. Wulan, Y. Li, Y. Zhang, J. Yan and Q. Jiang, *Adv. Mater.*, 2017, **29**, 1606550.
18 D. Bao, Q. Zhang, F. Meng, H. Zhong, M. Shi, Y. Zhang, J. Yan, Q. Jiang and X. Zhang, *Adv. Mater.*, 2017, **29**, 1604799.
19 H. Huang, L. Xia, X. Shi, A. M. Asiri and X. Sun, *Chem. Commun.*, 2018, **54**, 11427–11430.
20 H. Liu, S. Han, Y. Zhao, Y. Zhu, X. Tian, J. Zeng, J. Jiang, B. Xia and Y. Chen, *J. Mater. Chem. A*, 2018, **6**, 3211–3217.
21 C. Lv, C. Yan, G. Chen, Y. Ding, J. Sun, Y. Zhou and G. Yu, *Angew. Chem., Int. Ed.*, 2018, **57**, 6073–6076.
22 L. Zhang, X. Ren, Y. Luo, X. Shi, A. M. Asiri, T. Li and X. Sun, *Chem. Commun.*, 2018, **54**, 12966–12969.
23 S. Chen, S. Perathoner, C. Ampelli, C. Mebrahtu, D. Su and G. Centi, *Angew. Chem., Int. Ed.*, 2017, **56**, 2699–2703.
24 Q. Liu, X. Zhang, B. Zhang, Y. Luo, G. Cui, F. Xie and X. Sun, *Nanoscale*, 2018, **10**, 14386–14389.
25 J. Han, X. Ji, X. Ren, G. Cui, L. Li, F. Xie, H. Wang, B. Li and X. Sun, *J. Mater. Chem. A*, 2018, **6**, 12974–12977.
26 Z. Wang, F. Gong, L. Zhang, R. Wang, L. Ji, Q. Liu, Y. Luo, H. Guo, Y. Li, P. Gao, X. Shi, B. Li, B. Tang and X. Sun, *Adv. Sci.*, 2018, **5**, 1801182.
27 J. Du, X. Lai, N. Yang, J. Zhai, D. Kisailus, F. Su, D. Wang and L. Jiang, *ACS Nano*, 2011, **5**, 590–596.
28 W. Li, Y. Bai, F. Li, C. Liu, K. Chan, X. Feng and X. Lu, *J. Mater. Chem.*, 2012, **22**, 4025–4031.
29 J. Shao, W. Sheng, M. Wang, S. Li, J. Chen, Y. Zhang and S. Cao, *Appl. Catal., B*, 2017, **209**, 311–319.
30 W. Ren, Z. Ai, F. Jia, L. Zhang, X. Fan and Z. Zou, *Appl. Catal., B*, 2007, **69**, 138–144.
31 E. M. Neville, M. J. Mattle, D. Loughrey, B. Rajesh, M. Rahman, J. M. D. MacElroy, J. A. Sullivan and K. R. Thampi, *J. Phys. Chem. C*, 2012, **116**, 16511–16521.
32 B. Li, Z. Zhao, F. Gao, X. Wang and J. Qiu, *Appl. Catal., B*, 2014, **147**, 958–964.
33 C. Yang, X. Zhang, J. Qin, X. Shen, R. Yu, M. Ma and R. Liu, *J. Catal.*, 2017, **347**, 36–44.
34 Y. Zhang, Z. Zhao, J. Chen, L. Cheng, J. Chang, W. Sheng, C. Hu and S. Cao, *Appl. Catal., B*, 2015, **165**, 715–722.
35 C. Chen, M. Long, H. Zeng, W. Cai, B. Zhou, J. Zhang, Y. Wu, D. Ding and D. Wu, *J. Mol. Catal. A: Chem.*, 2009, **314**, 35–41.
36 C. D. Valentin, G. Pacchioni and A. Selloni, *Chem. Mater.*, 2005, **17**, 6656–6665.
37 D. Zhu, L. Zhang, R. E. Ruther and R. J. Hamers, *Nat. Mater.*, 2013, **12**, 836–841.
38 Y. Zhu, Y. Liu, T. Ren and Z. Yuan, *Adv. Funct. Mater.*, 2015, **25**, 7337–7347.
39 C. Guo, L. Zhang, J. Miao, J. Zhang and C. Li, *Adv. Energy Mater.*, 2013, **3**, 167–171.
40 Y. Liu, Y. Su, X. Quan, X. Fan, S. Chen, H. Yu, H. Zhao, Y. Zhang and J. Zhao, *ACS Catal.*, 2018, **8**, 1186–1191.
41 D. Yang, T. Chen and Z. Wang, *J. Mater. Chem. A*, 2017, **5**, 18967–18971.
42 J. Kong, A. Lim, C. Yoon, J. H. Jang, H. C. Ham, J. Han, S. Nam, D. Kim, Y. Sung, J. Choi and H. S. Park, *ACS Sustainable Chem. Eng.*, 2017, **5**, 10986–10995.
43 M. Shi, D. Bao, S. Li, B. Wulan, J. Yan and Q. Jiang, *Adv. Energy Mater.*, 2018, **8**, 1800124.
44 X. Xiang, Z. Wang, X. Shi, M. Fan and X. Sun, *ChemCatChem*, 2018, **10**, 1–7.
45 G. W. Watt and J. D. Chrisp, *Anal. Chem.*, 1952, **24**, 2006–2008.
46 R. Zhang, X. Ren, X. Shi, F. Xie, B. Zheng, X. Guo and X. Sun, *ACS Appl. Mater. Interfaces*, 2018, **10**, 28251–28255.
47 X. Zhang, Q. Liu, X. Shi, A. M. Asiri, Y. Luo, X. Sun and T. Li, *J. Mater. Chem. A*, 2018, **6**, 17303–17306.
48 R. Wang, Z. Wang, X. Xiang, R. Zhang, X. Shi and X. Sun, *Chem. Commun.*, 2018, **54**, 10340–10342.

